The Astrophysical Journal, 593:980–991, 2003 August 20

NONAXISYMMETRIC g-MODE AND p-MODE INSTABILITY IN A HYDRODYNAMIC THIN ACCRETION DISK

Li-Xin Li,[1,2] Jeremy Goodman,[3] and Ramesh Narayan[1]
Received 2003 March 11; accepted 2003 May 2

ABSTRACT

It has been suggested that quasi-periodic oscillations of accreting X-ray sources may relate to the modes named in the title. We consider nonaxisymmetric linear perturbations to an isentropic, isothermal, unmagnetized thin accretion disk. The radial wave equation, in which the number of vertical nodes (n) appears as a separation constant, admits a wave action current that is conserved except, in some cases, at corotation. Waves without vertical nodes amplify when reflected by a barrier near corotation. Their action is conserved. As was previously known, this amplification allows the $n = 0$ modes to be unstable under appropriate boundary conditions. In contrast, we find that waves with $n > 0$ are strongly absorbed at corotation rather than amplified; their action is not conserved. Therefore, nonaxisymmetric p-modes and g-modes with $n > 0$ are damped and stable even in an inviscid disk. This eliminates a promising explanation for quasi-periodic oscillations in neutron star and black hole X-ray binaries.

Subject headings: accretion, accretion disks — instabilities — waves — X-rays: binaries

1. INTRODUCTION

In recent years, the study of quasi-periodic oscillations (QPOs) in X-ray binaries has developed into a major field. A variety of QPOs have been observed in the variability power spectra of neutron star and black hole X-ray binaries (van der Klis 2000; Remillard et al. 2002 and references therein), and the observations have revealed a rich phenomenology.

Of particular interest are the "kilohertz QPOs," which have frequencies of several hundreds of Hz to occasionally more than 10^3 Hz. Because of their high frequencies, these QPOs must be produced by processes close to the accreting mass. However, since they have been seen in both neutron star and black hole X-ray binaries, it appears that the oscillations are not associated with the surface of the accreting object. Instead, it is generally believed that the kilohertz QPOs originate in the accretion flow surrounding the central mass.

A detailed understanding of the oscillation modes of accretion disks could in principle allow observations of QPOs to be used to test strong gravity in the vicinity of compact objects (e.g., Stella & Vietri 1998; Stella, Vietri, & Morsink 1999). Observations could also be "inverted" to measure relativistic parameters of the accreting mass, such as the spin of a black hole (Nowak et al. 1997; Wagoner, Silbergleit, & Ortega-Rodriguez 2001). However, such applications require a robust method of associating different observed QPO frequencies with specific disk modes and of calculating the frequencies of those modes from first principles.

In what follows, we focus on g-modes and p-modes in hydrodynamic thin disks. Following Silbergleit, Wagoner, & Ortega-Rodríguez (2001), Kato (2002), and references therein, we distinguish between the two kinds of modes primarily in terms of where most of the wave action is concentrated. If the bulk of the action is near corotation, we call it a g-mode, and if the action is mostly away from corotation, we call it a p-mode.

In an important paper, Okazaki, Kato, & Fukue (1987) showed that axisymmetric g-modes are trapped in the inner regions of a relativistic disk, where the epicyclic frequency κ reaches a maximum. This idea was exploited by Nowak & Wagoner (1991, 1992) and a number of other workers (Perez et al. 1997; Silbergleit et al. 2001; Abramowicz & Kluzniak 2001) who worked out the physical properties of these and related modes (for reviews see Kato, Fukue, & Mineshige 1998; Wagoner 1999; Kato 2001a). The modes are not dynamically unstable, however. Ortega-Rodriguez & Wagoner (2000) claim that viscosity destabilizes p- and g-modes, but we limit ourselves to inviscid disks.

Recently, Kato (2001b, 2002) claimed to demonstrate that *nonaxisymmetric* g-modes are trapped between two forbidden zones that lie on either side of the corotation radius. Kato further argued that these modes are highly unstable. This is very interesting because the observed kilohertz QPOs often have quite a large amplitude of flux variations, suggesting that the corresponding disk modes are probably dynamically unstable. This causes any disk modes that are dynamically unstable to be of great interest for the QPO problem. Although in a later paper Kato (2003) has withdrawn the claim of an instability, his work nevertheless suggests that it might be fruitful to explore dynamical instabilities in nonaxisymmetric disk modes. This is the motivation behind the present paper.

The work presented here is influenced by the papers of Goldreich & Narayan (1985, hereafter GN) and Narayan, Goldreich, & Goodman (1987, hereafter NGG). These authors studied perturbations in a particular simplified fluid system called the shearing sheet. They showed that nonaxisymmetric modes with no vertical nodes ($n = 0$ in the notation used in this paper) can be dynamically unstable.

[1] Harvard-Smithsonian Center for Astrophysics, 60 Garden Street, Cambridge, MA 02138; lli@cfa.harvard.edu, rnarayan@cfa.harvard.edu.
[2] Chandra Fellow.
[3] Princeton University Observatory, Princeton, NJ 08544; jeremy@astro.princeton.edu.

They further demonstrated that the driving force for the instability is a wave amplifier inside the system. These papers were in turn influenced by work on spiral wave amplification in stellar disks, especially Mark (1976).

We use the physical understanding obtained from the above work to guide our present investigation. In § 2 we consider a thin accretion disk (which is more general than the shearing sheet) and derive a wave equation for linear nonaxisymmetric perturbations and an associated conserved current. In § 3 we explore the nature of the singularities in the wave equation associated with the corotation resonance and the Lindblad resonances. In § 4 we consider the WKB limit of the wave equation and identify the basic properties of ingoing and outgoing waves in various regions of the disk. In § 5 we consider the interaction of waves with various barriers associated with the Lindblad and/or corotation resonance. We show that waves with $n = 0$ are amplified when they reflect off the corotation barrier. This confirms the result obtained by GN and NGG. However, when we repeat the analysis for waves with $n > 0$ (waves with one or more nodes in the vertical direction), we find that there is no amplifier anywhere in the system, either at the Lindblad resonances (§ 5) or at corotation (§ 6). Indeed, we show that corotation acts as a severe absorber of waves. Based on these results, we conclude in § 7 that there are no dynamically unstable p- or g-modes with $n > 0$ in a thin disk. Appendix A presents some numerical results that help to extend the analysis to the non-WKB regime, and Appendix B relates the corotation absorber studied here to some classical results concerning critical layers in stratified shear flows.

2. WAVE EQUATION FOR NONAXISYMMETRIC PERTURBATIONS TO A THIN DISK

We consider an axisymmetric thin disk. Because of the symmetry of the unperturbed system, we assume without loss of generality that the linear perturbations are proportional to $\exp[i(-\omega t + m\phi)]$ in cylindrical coordinates (r, ϕ, z). Here m is an integer and ω is the mode frequency, which may be either real or complex. We write the linear perturbations to the mass density and velocity as

$$\rho(t, r, \phi, z) = \rho_0(r, z) + \rho_1(r, z) \exp[i(-\omega t + m\phi)] , \quad (1)$$

$$v_r(t, r, \phi, z) = u(r, z) \exp[i(-\omega t + m\phi)] , \quad (2)$$

$$v_\phi(t, r, \phi, z) = \Omega(r) r + v(r, z) \exp[i(-\omega t + m\phi)] , \quad (3)$$

$$v_z(t, r, \phi, z) = w(r, z) \exp[i(-\omega t + m\phi)] , \quad (4)$$

where ρ_0 is the unperturbed mass density, Ω is the unperturbed angular velocity, and ρ_1, u, v, and w are first-order perturbations to the mass density and the velocity field. Note that $\partial\Omega/\partial z = 0$ since we take the disk to be isentropic. Following Kato, we use Newtonian equations. Although general relativity may introduce additional instabilities, many of its effects can be mimicked by appropriate radial variations of the structural disk frequencies Ω, κ, and $\Omega_\perp$, the latter two of which are defined below.

For simplicity, we assume that the disk has an isothermal equation of state,

$$p = \rho c_s^2 , \quad (5)$$

where p is the gas pressure and c_s is the sound speed, which we take to be a constant. The equilibrium structure of a sufficiently thin isothermal disk then takes the form

$$\rho_0(r, z) = \rho_{00}(r) \exp\left(-\frac{z^2}{2h^2}\right) , \quad (6)$$

where $h = h(r) = c_s/\Omega_\perp(r)$ is the half-thickness of the disk and $\Omega_\perp$ is the vertical disk frequency, which may be different from the orbital angular velocity as a result of strong radial pressure gradients in a Newtonian disk (unlikely for a thin disk) or relativistic gravity.

The isothermal equation of state allows an almost exact separation of variables, as shown below. This simplification is well worth the loss of generality, especially since the main focus of our paper is on the corotation resonance. In the vicinity of the corotation resonance, in fact, the frequency σ (defined below) is small compared to the reciprocal of the sound crossing time across the thickness of the disk; consequently, motions near corotation are noncompressive, so that the choice among different isentropic equations of state is not important. Far from corotation ($|r - r_c| \gtrsim r/m$), however, non-isothermal equilibria concentrate waves toward the disk surface where they may be more easily dissipated (Bate et al. 2002 and references therein).

In terms of the enthalpy perturbation

$$Q = \frac{\delta p}{\rho_0} , \quad (7)$$

the first-order perturbation to the continuity equation is

$$\frac{1}{r\rho_0}\frac{\partial}{\partial r}(r\rho_0 u) + \frac{im}{r} v + \frac{1}{\rho_0}\frac{\partial}{\partial z}(\rho_0 w) = \frac{i\sigma}{c_s^2} Q , \quad (8)$$

where

$$\sigma \equiv \omega - m\Omega \quad (9)$$

is the frequency of the perturbation in the local corotating frame of the disk. The first-order perturbations to the radial, azimuthal, and vertical momentum equations lead to

$$i\sigma u + 2\Omega v = \frac{\partial Q}{\partial r} , \quad (10)$$

$$\frac{\kappa^2}{2\Omega} u - i\sigma v = -\frac{im}{r} Q , \quad (11)$$

$$i\sigma w = \frac{\partial Q}{\partial z} , \quad (12)$$

respectively, where

$$\kappa \equiv \sqrt{2\Omega\left(2\Omega + r\frac{d\Omega}{dr}\right)} \quad (13)$$

is the epicyclic frequency of the flow in the (r, ϕ)-plane.

Solving for u and v from equations (10) and (11) and for w from equation (12) and substituting the results into equation (8), we obtain a second-order partial differential equation for Q,

$$\frac{\sigma^2}{\rho_0 r}\frac{\partial}{\partial r}\left(\frac{\rho_0 r}{D}\frac{\partial Q}{\partial r}\right) - \left[\frac{\sigma^2}{c_s^2} + \left(\frac{m\sigma}{r}\right)^2 \frac{1}{D} + \frac{2m\sigma}{\rho_0 r}\frac{\partial}{\partial r}\left(\frac{\rho_0\Omega}{D}\right)\right] Q = \frac{1}{\rho_0}\frac{\partial}{\partial z}\left(\rho_0 \frac{\partial Q}{\partial z}\right) , \quad (14)$$

where

$$D \equiv \kappa^2 - \sigma^2 \ . \tag{15}$$

Equation (14) is most easily analyzed by separation of variables in r, z, as discussed by Kato (2001a). Since $dh/dr \sim h/r$ is small for a thin disk, we neglect the dependence of h on r and introduce a coordinate $\eta \equiv z/(\sqrt{2}h)$ to replace z. Then, writing $Q(r, \eta) = Q_r(r)Q_\eta(\eta)$ and substituting in equation (14), we can show that $Q_r(r)$ and $Q_\eta(\eta)$ satisfy

$$\frac{d}{dr}\left(\frac{\rho_{00} r}{D}\frac{dQ_r}{dr}\right) + \frac{\rho_{00} r}{\sigma^2} \times \left[\frac{n\Omega_\perp^2 - \sigma^2}{c_s^2} - \frac{m^2\sigma^2}{r^2 D} - \frac{2m\sigma}{\rho_{00} r}\frac{d}{dr}\left(\frac{\rho_{00}\Omega}{D}\right)\right] Q_r = 0 \ , \tag{16}$$

$$\frac{d^2 Q_\eta}{d\eta^2} - 2\eta\frac{dQ_\eta}{d\eta} + 2nQ_\eta = 0 \ , \tag{17}$$

where n is a constant.

Equation (17) has the form of the Hermite equation. In order for the energy density of perturbations to be bound as $\eta \to \pm\infty$, n must be a nonnegative integer (Okazaki et al. 1987): $n = 0, 1, 2, \ldots$. Then the solutions to equation (17) are given by the Hermite polynomials: $Q_\eta = H_n(\eta)$. The integer n determines the number of nodes in the vertical direction. An even (odd) n corresponds to an even (odd) mode of oscillation. The mode with $n = 0$ has $Q_\eta = \text{const}$ and has no motions in the vertical direction according to equation (12).

Equation (16), with $n = 0, 1, 2, \ldots$, is the wave equation for linear perturbations of an isothermal thin disk. Kato (2001a) obtained a similar equation for more general equations of state by neglecting slowly radially varying terms.

The quantity

$$J \equiv \frac{i}{2W}\left(Q_r^* \frac{dQ_r}{dr} - Q_r \frac{dQ_r^*}{dr}\right), \quad W \equiv \frac{D}{\rho_{00} r} \ , \tag{18}$$

where the asterisks denote complex conjugates, represents a current of wave action. It can be checked that this current is conserved, that is, $dJ/dr = 0$, wherever equation (16) is nonsingular and ω is real. The current plays a prominent role in all of the analysis presented below. The conservation law for wave action can be extended to complex frequencies $\omega = \omega_R + i\omega_I$,

$$-\frac{dJ}{dr} = 2\omega_I \rho_a \ ,$$

where ρ_a is a real quantity proportional to $|Q_r|^2$ representing the density of wave action (NGG). The role of the singularities is more important in the present context. We shall show that J is conserved at all singularities except corotation, and even there it is conserved when $n = 0$.

3. COROTATION AND LINDBLAD SINGULARITIES IN THE WAVE EQUATION

When σ is real (i.e., ω is real), the wave equation (16) contains two types of singularities: one is the corotation singularity given by the condition $\sigma = 0$, and the other is the Lindblad singularities given by the condition $D = 0$. The former occurs at the corotation radius r_c and the latter at the Lindblad radii r_L.

3.1. *Corotation Singularity: $n = 0$*

We begin by first discussing the case $n = 0$, which corresponds to the problem analyzed by GN and NGG. They considered the special case of the shearing sheet, whereas we consider here a more general disk; however, near corotation, the two problems are very similar. For r close to r_c, the wave equation becomes

$$\frac{d^2 Q_r}{dr^2} - \frac{A_c Q_r}{r_c(r - r_c)} = 0 \ ,$$
$$A_c \equiv \left[\frac{2}{-d\ln\Omega/d\ln r}\frac{d}{d\ln r}\ln\left(\frac{\rho_{00}\Omega}{D}\right)\right]_{r=r_c} , \tag{19}$$

where we have used $\sigma = m(-d\Omega/dr)_{r=r_c}(r - r_c)$ near $r = r_c$. Assuming that $Q_r \propto (r - r_c)^{\beta_1}$ near $r = r_c$, the leading term in equation (19) gives rise to

$$\beta_1(\beta_1 - 1)(r - r_c)^{\beta_1 - 2} = 0 \ , \tag{20}$$

which requires $\beta_1 = 0$ or 1. Thus, near the corotation radius the solutions to the wave equation are

$$Q_r \propto 1, \quad r - r_c \ . \tag{21}$$

Equation (21) implies that the solutions are analytic near $r = r_c$. Correspondingly, as can be easily checked, the current defined by equation (18) is conserved across r_c, i.e.,

$$\frac{J_{c-}}{J_{c+}} = 1, \quad J_{c\pm} \equiv J\left(r - r_c = 0^\pm\right) \ . \tag{22}$$

Therefore, when $n = 0$, there is no real singularity at corotation, only an apparent singularity. Indeed, for the model of a shearing sheet, NGG have shown that the corotation singularity does not appear at all if the perturbation equation is written in terms of the azimuthal velocity rather than Q_r.

3.2. *Corotation Singularity: $n > 0$*

When $n > 0$, the wave equation near the corotation radius becomes

$$\frac{d^2 Q_r}{dr^2} + \frac{nb^2 Q_r}{(r - r_c)^2} = 0, \quad b \equiv \left.\frac{\Omega_\perp \kappa}{mc_s(-d\Omega/dr)}\right|_{r=r_c} . \tag{23}$$

The solutions to equation (23) are

$$Q_r \propto (r - r_c)^{1/2 \pm 2iq}, \quad q \equiv \tfrac{1}{2}\sqrt{nb^2 - \tfrac{1}{4}} \ . \tag{24}$$

Because of the presence of the factor $(r - r_c)^{1/2}$, the solutions are not analytic at $r = r_c$. Thus, we have a real singularity. Note that, for a thin disk, we usually have $b \sim r/mh \gg 1$ unless m is $\gtrsim r/h$, so generally we expect $q \gg 1$.

Substituting the two solutions in equation (24) into equation (18), we can calculate the corresponding current density J_{c+} defined in the previous subsection. Making the analytic continuation $r - r_c \to (r - r_c)e^{\pi i}$ to the solutions in equation (24) and substituting the results into equation (18), we can calculate the corresponding current J_{c-}. We find that

the current is not conserved across corotation:

$$\left|\frac{J_{c-}}{J_{c+}}\right| = e^{\mp 4\pi q} , \tag{25}$$

where the upper/lower sign corresponds to the upper/lower sign in equation (24).

This analysis shows that the behavior near corotation is very different for $n = 0$ and $n > 0$. This is one of two major differences between the two cases, the other being the geometry of permitted and forbidden zones for waves, discussed in § 4 and displayed in Figures 1 and 2.

3.3. *Lindblad Singularity*

The Lindblad singularity occurs at the radii $r_{\rm L}$ where $D = 0$. Near this singularity, we have $\sigma \approx \pm\kappa$ and $D \approx D'_{\rm L}(r - r_{\rm L})$, assuming that $D'_{\rm L} \equiv (dD/dr)_{r=r_{\rm L}} \neq 0$. Then, assuming that $Q_r \propto (r - r_{\rm L})^{\beta_2}$ near $r = r_{\rm L}$, the leading term in equation (16) gives rise to

$$\beta_2(\beta_2 - 2)(r - r_{\rm L})^{\beta_2 - 3} = 0 , \tag{26}$$

which requires $\beta_2 = 0$ or 2. Thus, when $D'_{\rm L} \neq 0$, the two solutions to the wave equation are locally

$$Q_r \propto 1, \quad (r - r_{\rm L})^2 . \tag{27}$$

Both solutions are clearly analytic.

More generally, if D is an analytic function of r near the Lindblad radius (as it is in our problem), the solutions to the wave equation must also be analytic there. It can be checked that the current defined by equation (18) is then conserved across the Lindblad singularity. Therefore, the Lindblad resonance is not a true singularity but only an apparent singularity (NGG; Kato 2002). This is self-evident when the second-order equation (19) is replaced by the equivalent system of first-order equation (A12). Indeed, if one considers wave equations for other perturbed quantities (e.g., radial velocity), the Lindblad singularity gives way to other singular terms, which occur at different radii and are again not real singularities but only apparent. The corotation singularity, on the other hand, persists for any fluid variable one selects and is a genuine singularity when $n > 0$.

In summary, when $n > 0$, the corotation resonance is an intrinsic singularity in the wave equation, where the conservation of the current breaks down. When $n = 0$, the corotation resonance is only an apparent singularity; the solutions are well behaved there and the current is conserved across the resonance. The Lindblad resonance is never a real singularity; the solutions are well behaved and the current is conserved across the Lindblad resonance for all values of n.

4. WKB SOLUTIONS TO THE WAVE EQUATION IN PERMITTED REGIONS

In the WKB regime, where the wavelength is much smaller than the length scale over which the potential in the wave equation varies, the wave equation (16) can be approximated by

$$\frac{d^2 Q_r}{dr^2} - \frac{d\ln W}{dr}\frac{dQ_r}{dr} + k_r^2(r) Q_r = 0 , \tag{28}$$

where

$$k_r^2(r) \equiv \frac{\left(\sigma^2 - n\Omega_\perp^2\right)\left(\sigma^2 - \kappa^2\right)}{c_s^2 \sigma^2} . \tag{29}$$

In the last step, we have assumed that $mh/r \ll 1$. Equation (28) is Kato's (2001b, 2002) wave equation, except that we have retained the subdominant term involving the Wronskian W (eq. [18]). This term is crucial because it influences the sign of the wave action and hence the amplification of waves.

When the condition

$$\left|\frac{1}{k_r^2}\frac{dk_r}{dr}\right| \sim \left|\frac{1}{k_r r}\right| \ll 1 \tag{30}$$

is satisfied, the wave equation (28) can be solved with the WKB approximation (see, e.g., Merzbacher 1998):

$$Q_{r,\rm WKB} \approx \sqrt{\frac{W}{k_r}} \exp\left(\pm i \int^r k_r \, dr\right) . \tag{31}$$

The solution with the plus sign in the exponential corresponds to wavevector $+k_r$, and the solution with the minus sign corresponds to wavevector $-k_r$.

Within the WKB approximation, permitted regions for waves are defined by the requirement $k_r^2(r) > 0$, and forbidden regions by $k_r^2(r) < 0$. Consider first the simpler case of $n = 0$. Here the region of the disk in which $\sigma^2 < \kappa^2$ is forbidden. This region extends from the inner Lindblad radius ($\sigma = -\kappa$) to the outer Lindblad radius ($\sigma = \kappa$), straddling the corotation radius ($\sigma = 0$). It is shown as forbidden region A in Figure 1. On either side of A, there are two permitted regions: region I with $\sigma < -\kappa$ and region II with $\sigma > \kappa$.

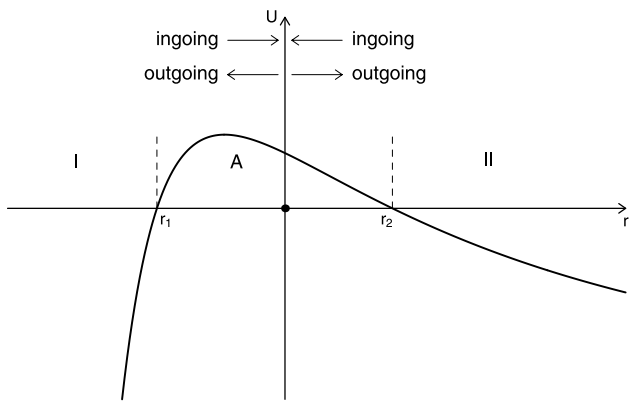

FIG. 1.—Potential $U(r) \equiv -k_r^2(r)$ in the wave eq. (28) for the case in which $n = 0$. There are two permitted regions and one forbidden region along the r-axis. The two permitted regions are I ($r < r_1$) and II ($r > r_2$), where r_1 and r_2 are defined by $\sigma = \mp\kappa$. The boundaries of the regions are marked by the two vertical dashed lines. The forbidden region is A ($r_1 < r < r_2$), which contains the corotation radius as marked by the dot. (When $n = 0$, the corotation radius is not a singularity in the wave eq. [28].) The directions of ingoing and outgoing waves are shown with horizontal arrows, which are defined relative to the corotation radius. The relations among the directions of the current, the wavevector, and the group velocity in each permitted region are summarized in Table 1.

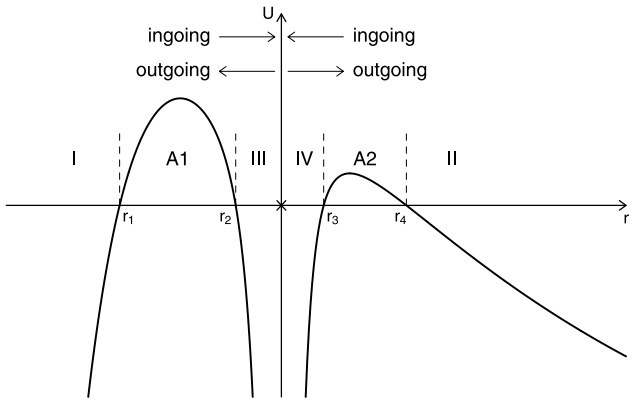

FIG. 2.—Potential $U(r) \equiv -k_r^2(r)$ in the wave eq. (28) for the case in which $n > 0$. There is an intrinsic singularity at the corotation radius at $r = r_c$ where $\sigma = 0$ and the potential is infinitely deep, as indicated by the cross. There are four permitted regions and two forbidden regions along the r-axis. The permitted regions are I ($r < r_1$), II ($r > r_4$), III ($r_2 < r < r_c$), and IV ($r_c < r < r_3$), where r_1 and r_4 are defined by $\sigma = \mp \max(\sqrt{n}\Omega_\perp, \kappa)$ and r_2 and r_3 are defined by $\sigma = \mp \min(\sqrt{n}\Omega_\perp, \kappa)$. The boundaries of the regions are marked by the four vertical dashed lines plus the U-axis. The forbidden regions are A1 ($r_1 < r < r_2$) and A2 ($r_3 < r < r_4$). The directions of ingoing and outgoing waves are shown with horizontal arrows, which are defined relative to the corotation radius. The relations among the directions of the current, the wavevector, and the group velocity in each permitted region are summarized in Table 1.

When $n > 0$, things are more complicated. Now, there are four permitted regions (see Fig. 2):

Region I: the region with $\sigma < -\max(\sqrt{n}\Omega_\perp, \kappa)$.
Region II: the region with $\sigma > \max(\sqrt{n}\Omega_\perp, \kappa)$.
Region III: the region with $-\min(\sqrt{n}\Omega_\perp, \kappa) < \sigma < 0$.
Region IV: the region with $0 < \sigma < \min(\sqrt{n}\Omega_\perp, \kappa)$.

Regions I and III have $\sigma < 0$ and are on the left-hand side of corotation. These two zones are separated from each other by a forbidden zone (barrier A1; see Fig. 2). Regions II and IV have $\sigma > 0$ and are on the right-hand side of corotation. They are again separated from each other by a forbidden zone (barrier A2). Regions III and IV are separated from each other by the corotation resonance, which is not a true barrier. In contrast to the $n = 0$ case, here the region around corotation is permitted.

For a WKB solution with a wavevector k_r (i.e., the solution in eq. [31] with the plus sign in the exponential), the corresponding current is

$$J_{\rm WKB} \approx \frac{k_r}{-W} \left| Q_{r,\rm WKB} \right|^2 , \tag{32}$$

where we have used the fact that in the permitted regions k_r is real so that $k_r^* = k_r$. From the definition of W (eq. [18]), the sign of W is determined by the sign of $D = \kappa^2 - \sigma^2$. Hence, the current and the wavevector have the same signs in regions where $\sigma^2 > \kappa^2$ (regions I and II; see Table 1) but opposite signs where $\sigma^2 < \kappa^2$ (regions III and IV).

We now define an "outgoing" wave as one that moves away from corotation, i.e., toward larger $|\sigma|$, and an "ingoing" wave as one that moves toward corotation (see Figs. 1 and 2). The direction of motion is determined by the sign of the group velocity $v_{\rm gr}$ rather than the wavevector k_r.

By definition, $v_{\rm gr} \equiv (\partial k_r/\partial\omega)^{-1} = (\partial k_r/\partial\sigma)^{-1}$, so that

$$k_r v_{\rm gr} = \sigma \left(\frac{\partial \ln k_r^2}{\partial \ln \sigma^2} \right)^{-1} . \tag{33}$$

TABLE 1

RELATIONS AMONG THE DIRECTIONS OF THE CURRENT, THE WAVEVECTOR, AND THE GROUP VELOCITY IN THE FOUR PERMITTED REGIONS

Region	$D \equiv \kappa^2 - \sigma^2$	$k_r J$[a]	$k_r v_{\rm gr}$[b]	$v_{\rm gr} J$[c]
I	−	+	−	−
II.....	−	+	+	+
III	+	−	+	−
IV	+	−	−	+

NOTE.—When $n = 0$, regions III and IV disappear (see § 4).

[a] The sign of the product $k_r J$ determines the relative directions between the current J and the wavevector k_r.

[b] The sign of the product $k_r v_{\rm gr}$ determines the relative directions between the wavevector k_r and the group velocity $v_{\rm gr}$.

[c] The sign of the product $v_{\rm gr} J$ determines the relative directions between the current J and the group velocity $v_{\rm gr}$.

From equation (29) we have

$$\frac{\partial \ln k_r^2}{\partial \ln \sigma^2} = \frac{\sigma^4 - n\Omega_\perp^2 \kappa^2}{(\sigma^2 - n\Omega_\perp^2)(\sigma^2 - \kappa^2)} , \tag{34}$$

and therefore

$$k_r v_{\rm gr} = \frac{c_s^2 k_r^2 \sigma^3}{\sigma^4 - n\Omega_\perp^2 \kappa^2} . \tag{35}$$

It is then easily verified that $k_r v_{\rm gr} > 0$ in regions II and III and $k_r v_{\rm gr} < 0$ in regions I and IV. This allows us to identify whether a particular wave in a given permitted region is ingoing or outgoing.

Knowing the signs of $k_r J$ and $k_r v_{\rm gr}$ in each permitted region, we are able to determine the sign of $v_{\rm gr} J$ in that region (Table 1). This is an important quantity, as we show in the next section.

Finally, we briefly comment on the locations of the four permitted regions in a real disk. From their definitions, if all four regions I, II, III, and IV exist, they should appear in the following order with increasing disk radius (as in Fig. 2): region I, region III, region IV, and region II, since σ is an increasing function of radius. Thus, we expect region I to be near the inner boundary of the disk ($r \approx r_{\rm in}$), region II to be at large radii ($r \gg r_c$), and regions III and IV to lie in between, on either side of corotation.

5. WAVE AMPLIFICATION/DEAMPLIFICATION AT THE BARRIERS

As explained in § 1, a dynamical instability is possible if there is a wave amplifier in the system. In the case of $n = 0$, such an amplifier is present at the corotation barrier (GN; NGG), as we now demonstrate using the results derived in § 4. Figure 1 shows that, when $n = 0$, there are only two permitted regions in the disk: region I near the inner boundary of the disk, and region II at large radii. These two regions are separated from each other by barrier A, which includes the corotation and Lindblad resonances. However, as shown in §§ 3.1 and 3.3, neither the corotation resonance nor the Lindblad resonances are real singularities, and the current defined by equation (18) is conserved throughout the disk.

Consider now a wave incident on the potential barrier from region I. The interaction of this ingoing wave with the potential barrier will produce a reflected outgoing wave in region I and a transmitted outgoing wave in region II. Because of the conservation of the current, we have the following relation among the currents of the three waves:

$$J_{\rm in}^{\rm (I)} + J_{\rm out}^{\rm (I)} = J_{\rm out}^{\rm (II)} \ . \tag{36}$$

From Table 1, in region II the group velocity and the current density of the wave have the same sign. Since an outgoing wave in region II has a positive group velocity (the wave goes away from corotation toward larger r), the corresponding current $J_{\rm out}^{\rm (II)}$ must be positive. Thus, the right-hand side of equation (36) is positive. In region I, the group velocity and the current of the wave have opposite signs. The ingoing wave here has a positive group velocity (it is moving from small values of r toward r_c), while the outgoing wave has a negative group velocity. Thus, $J_{\rm in}^{\rm (I)} < 0$ and $J_{\rm out}^{\rm (I)} > 0$. Then, equation (36) is equivalent to

$$\left|J_{\rm out}^{\rm (I)}\right| = \left|J_{\rm in}^{\rm (I)}\right| + \left|J_{\rm out}^{\rm (II)}\right| \ . \tag{37}$$

We define the *gain* G to be the absolute value of the reflection coefficient. Equation (37) implies that the gain

$$G \equiv \left|\frac{J_{\rm reflected}}{J_{\rm incident}}\right| = \left|\frac{J_{\rm out}^{\rm (I)}}{J_{\rm in}^{\rm (I)}}\right| > 1, \quad n = 0 \ . \tag{38}$$

In other words, for $n = 0$, an incident wave is reflected by the potential barrier with a larger amplitude, and the potential barrier behaves as an amplifier. If, in addition, the inner edge of the disk behaves like a near-perfect reflector, then we have the makings of an instability. (This would be a p-mode disk instability since the wave action is concentrated away from corotation.)

The corotation amplifier works equally well if a wave is incident on the potential barrier from region II, as is easily verified. In this case, to have an instability, the outgoing wave in region II must be somehow reflected. The reflection is unlikely to be from the distant outer edge of the disk. Perhaps an inhomogeneity in the disk might provide the necessary reflection, but the topic is beyond the scope of this paper. For the purposes of this paper, the key point is that, when $n = 0$, the system has a wave amplifier and, therefore, can potentially have unstable modes.

The situation changes dramatically when $n > 0$. Now, there are four permitted regions in the disk, I, II, III, and IV, and two barriers, A1 and A2. Let us consider the region to the right of corotation (i.e., $\sigma > 0$). Assume that an outgoing wave is incident on the barrier A2 from region IV. The interaction of this outgoing wave with the barrier produces a reflected ingoing wave in region IV and a transmitted outgoing wave in region II. We have shown earlier that there is no real singularity at the barrier, and so the current density must be conserved from region IV to region II. We then have

$$J_{\rm out}^{\rm (IV)} + J_{\rm in}^{\rm (IV)} = J_{\rm out}^{\rm (II)} \ . \tag{39}$$

From Table 1 we see that in region IV the group velocity and the current have the same sign. Since in region IV an outgoing wave has a positive group velocity and an ingoing wave has a negative group velocity, we have $J_{\rm out}^{\rm (IV)} > 0$ and $J_{\rm in}^{\rm (IV)} < 0$. Similarly, $J_{\rm out}^{\rm (II)} > 0$. Thus, equation (39) can be rewritten as

$$\left|J_{\rm in}^{\rm (IV)}\right| = \left|J_{\rm out}^{\rm (IV)}\right| - \left|J_{\rm out}^{\rm (II)}\right| \ . \tag{40}$$

Equation (40) implies that the gain in this case is always less than unity:

$$G = \left|\frac{J_{\rm reflected}}{J_{\rm incident}}\right| = \left|\frac{J_{\rm in}^{\rm (IV)}}{J_{\rm out}^{\rm (IV)}}\right| < 1, \quad n > 0 \ . \tag{41}$$

In other words, a wave that is incident on barrier A2 from region IV is always reflected with a smaller amplitude. It can be easily checked that this statement is true also for a wave incident on barrier A2 from region II and also for waves incident on barrier A1 from either region I or region III.

We thus conclude that, for $n > 0$, neither of the two barriers A1 and A2 behaves like an amplifier; both barriers deamplify waves. This eliminates a promising mechanism for producing a dynamical nonaxisymmetric instability. The only thing left to be checked is whether corotation itself can amplify waves. This is the topic of the next section.

6. ABSORPTION AT THE COROTATION RESONANCE

To understand the role played by the corotation singularity when $n > 0$, we need to study the behavior of the solutions of the wave equation (16) near $\sigma = 0$ (i.e., $r = r_c$). In particular, we would like to know, for a wave incident on the resonance, how much is transmitted to the other side and how much is reflected.

As $|\sigma| \to 0$ (i.e., $r \to r_c$), and taking $n > 0$, the wave equation becomes equation (23), whose two linearly independent solutions are given by equation (24) for $q \neq 0$. The wavevectors corresponding to the two solutions are

$$k_r = \pm \frac{\sqrt{n}b}{r - r_c} \ . \tag{42}$$

It can be checked that when $\sqrt{n}b \gg 1$ (i.e., $q \gg 1$) the solutions in equation (24) become the WKB solutions given by equation (31).

According to Table 1, in region IV ($r > r_c$) the wavevector and the group velocity have opposite signs. Thus, in region IV the ingoing wave, which has a negative group velocity, i.e., a positive wavevector, is given by $(r - r_c)^{1/2+2iq}$. Now let us analytically continue this solution into region III. As discussed in NGG, the continuation must be done such that the integration path in the complex plane goes above the singularity at $\sigma = 0$ if the solution is to correspond to an initial-value problem. That is, we must take $r - r_c \to |r - r_c| e^{\pi i}$. We then find that the solution transforms as follows:

$$\text{region IV} \to \text{region III}: \ (r - r_c)^{1/2+2iq} \to i e^{-2\pi q} |r - r_c|^{1/2+2iq} \ . \tag{43}$$

In region III ($r < r_c$) the wavevector and the group velocity have the same sign. Hence, in region III the outgoing wave, which has a negative group velocity, i.e., a negative wavevector, is given by $(r - r_c)^{1/2+2iq} \propto |r - r_c|^{1/2+2iq}$. Thus, from equation (43), the ingoing wave in region IV becomes a purely outgoing wave with a reduced amplitude in region III, and there is no reflected wave.

Similarly, for an ingoing wave in region III we find

$$\text{region III} \rightarrow \text{region IV}: \quad (r_c - r)^{1/2-2iq} \rightarrow -ie^{-2\pi q}|r - r_c|^{1/2-2iq}, \quad (44)$$

where we have taken $r_c - r \rightarrow |r - r_c|e^{-\pi i}$.

Computing currents, we may calculate the transmission and reflection coefficients T_c and R_c of the corotation resonance:

$$T_c = e^{-4\pi q}, \quad R_c = 0. \quad (45)$$

Thus, there is no wave reflection at the corotation singularity, and there is a severe absorption of wave action in the transmitted wave. Indeed, the absorption is exponentially strong when q is large (as for a thin disk).

From equation (45), it might appear that the absorption would disappear for $nb^2 \leq \frac{1}{4}$ since then q becomes zero or imaginary and so $|T_c| = 1$. However, this is not true in general, and absorption disappears only when $nb^2 = 0$ (i.e., $q = \pm i/4$). For example, consider a solution in region IV containing both ingoing and outgoing waves,

$$Q_r^{(\mathrm{IV})} = A_1(r - r_c)^{1/2+2iq} + A_2(r - r_c)^{1/2-2iq}, \quad (46)$$

where A_1 and A_2 are complex numbers. The corresponding solution in region III obtained by analytic continuation is

$$Q_r^{(\mathrm{III})} = iA_1e^{-2\pi q}|r - r_c|^{1/2+2iq} + iA_2e^{2\pi q}|r - r_c|^{1/2-2iq}. \quad (47)$$

Then we can calculate the net currents on the two sides of corotation. We find

$$\frac{J_{\mathrm{in}}^{(\mathrm{IV})} + J_{\mathrm{out}}^{(\mathrm{IV})}}{J_{\mathrm{in}}^{(\mathrm{III})} + J_{\mathrm{out}}^{(\mathrm{III})}} = -\frac{1}{\cos 4\pi\bar{q} + \cot\psi \sin 4\pi\bar{q}}, \quad (48)$$

where $\bar{q} \equiv iq$ and $2\psi \equiv \arg(A_1A_2^*/A_1^*A_2)$. The ratio of the currents is equal to 1 for any ψ if and only if $q = \pm i/4$, i.e., $nb^2 = 0$ (in which case the corotation singularity disappears or becomes an apparent singularity and we return to the case studied by NGG). Thus, we conclude that, in general, nonaxisymmetric g-modes in disks are absorbed at corotation. In other words, the corotation singularity deamplifies waves and therefore cannot induce an instability.

Absorption at corotation is not unique to disk g-modes. It occurs for other sorts of waves in shear flows and has been well studied in the fluid dynamics literature. Appendix B contains references to this literature and some other ways of understanding the corotation resonance.

Combined with the results in § 5, we see that, when $n > 0$, there are no amplifiers in the system, either at the two barriers or at corotation, and so there are no nonaxisymmetric growing modes trapped in the disk. This result has been obtained here via a WKB analysis. We confirm the result in Appendix A with numerical calculations for the specific case of the shearing sheet model. That analysis is more general and goes beyond the WKB approximation.

7. SUMMARY AND DISCUSSION

We have derived the wave equation for nonaxisymmetric perturbations in an isothermal hydrodynamic thin disk and have identified a conserved current (§ 2). The wave equation contains two types of singularities: the corotation singularity and the Lindblad singularity. The Lindblad singularity is never a real singularity, regardless of the vertical wavenumber n; the solutions are always analytic and well behaved in the vicinity of this singularity, and the current is conserved across it (§ 3). For $n = 0$ (horizontal motions independent of height), corotation is also not a real singularity, and the current is conserved. However, for waves having vertical nodes ($n > 1$), corotation is a true singularity where the conservation of current breaks down.

Using a WKB approach (§ 4), we have shown that for $n = 0$ there are two permitted regions in the disk (Fig. 1), one near the inner boundary (region I) and the other at large radii (region II). In contrast, for the first and higher overtones ($n > 0$), there are four permitted regions in the disk (Fig. 2): region I near the inner boundary, region II at large radii, and regions III and IV in between, on either side of corotation. We have analyzed the WKB solutions in each permitted region, mapped the ingoing and outgoing waves, and identified the signs of the current density and group velocity of the various waves (summarized in Table 1).

For $n = 0$, the current is conserved throughout the entire disk, from the inner boundary to infinity. This, combined with the results given in Table 1, allows us to demonstrate that the disk behaves like a wave amplifier (§ 5). The argument is simple. We consider an ingoing wave in region I, which produces a reflected outgoing wave in region I and a transmitted outgoing wave in region II. Since the outgoing wave in region II has a positive current, by the conservation of current, this means that the sum of the ingoing and outgoing waves in region I should also have a positive current. However, in region I, the outgoing wave has a positive current and the ingoing wave has a negative current. Thus, the outgoing wave in region I must have a larger amplitude than the ingoing wave. In other words, the interaction of the ingoing wave with the corotation region has caused wave amplification in the reflected outgoing wave.

This result for $n = 0$ waves was shown for the case of the shearing sheet model by GN and NGG. Indeed, these authors showed that the amplifier causes an instability if a reflecting boundary condition exists in one of the permitted regions. The reflective boundary causes the amplified outgoing wave to return to corotation and be amplified repeatedly. While this instability is a candidate to explain QPOs in accretion systems, it unfortunately requires nearly perfect reflection at the boundary, presumably the inner edge of the disk, which is somewhat problematic. As the analytical results in the above-quoted papers indicate, and also confirmed in the numerical calculations of Appendix A of the present paper (see the first two rows of Table 2), the amplifi-

TABLE 2

NUMERICAL SOLUTIONS FOR GAIN AND TRANSMISSION FOR THE SHEARING SHEET MODEL

n	$\Omega_\perp/\Omega_c$	κ/Ω_c	k_yh	G[a]	T[b]	Amplification[c]
0.....	1.0	1.0	0.3	1.000496	4.96E−4	√
	1.0	1.1	0.4	1.000447	4.47E−4	√
	0.8	0.2	0.3	1.524428	5.24E−1	√
1.....	1.0	1.0	0.3	3.89E−1	4.60E−7	×
	1.0	1.1	0.4	4.94E−1	1.60E−6	×
	0.8	0.2	0.3	9.38E−1	7.63E−3	×

[a] The gain, i.e., the reflection coefficient, defined by eq. (A13).

[b] The transmission coefficient defined by eq. (A14).

[c] Amplification ($G > 1$) is marked with "√"; deamplification ($G < 1$) is marked with a cross.

cation at the corotation barrier is usually extremely weak for a thin disk. Thus, any energy loss either during transit of the wave to the boundary and back or during the reflection at the boundary would kill the instability. The requirement of perfect reflection at the boundary is particularly troublesome, since Blaes (1987) has shown that any radial inflow of the gas at the boundary (which is unavoidable in an accretion flow) would severely reduce the reflectivity of the boundary.

What is needed is a sufficiently strong amplifier, such that even less than perfect reflection at the boundary is sufficient to give overall amplification and instability. Kato's (2001b, 2002) claim that nonaxisymmetric g-modes with $n > 0$ are strongly amplified appeared to be just the answer. Unfortunately, Kato (2003) himself discovered that g-modes do not grow, and our independent analysis described in this paper confirms his result. We have shown in § 4 that for first and higher overtone modes ($n > 0$), there are two barriers, one near each Lindblad resonance, instead of the single barrier for the $n = 0$ case (compare Figs. 1 and 2). Both barriers unfortunately behave as wave deamplifiers rather than amplifiers (§ 5); for a wave that is incident on either barrier from either side, both the reflected wave and the transmitted wave are weaker than the original wave (the total current is, however, conserved). Furthermore, for these $n > 0$ waves, the corotation singularity behaves as a strong wave absorber (§ 6) so that current is absorbed and is lost whenever a wave is incident on corotation. Thus, we conclude that $n > 0$ modes are unable to grow in a thin disk.

If we define g-modes as those that have the bulk of their wave action near corotation (Silbergleit et al. 2001; Kato 2002), then these modes must of necessity have $n > 0$, since only such modes have a permitted region near corotation (Fig. 2). Our analysis thus shows that nonaxisymmetric g-modes cannot be dynamically unstable. The p-modes, which have their wave action far away from corotation, are possible for both $n = 0$ and $n > 0$. Unstable $n > 0$ p-modes are again ruled out by our analysis. This leaves only the $n = 0$ modes, which we discussed earlier, as candidates for QPOs. We have already argued that these modes are unlikely to grow in thin disks. Perhaps with a sufficiently thick disk, the wave amplifier could become strong (e.g., see the third row in Table 2) and might give an instability, but this is not very promising since it is likely that a thick disk will also have more rapid gas inflow at the inner boundary and therefore weaker reflection there.

Perhaps by adding more physics to the disk model one may yet find a global hydrodynamic instability suited to explain QPOs. As already noted, axisymmetric *viscous* instabilities have been proposed by Ortega-Rodriguez & Wagoner (2000). Vertical stratification (i.e., perpendicular to the mean flow) may allow nonaxisymmetric instability in some laboratory Couette flows (Yavneh, McWilliams, & Molemaker 2001). In our opinion, neither of these is a very plausible instability mechanism for disks, but space does not permit an adequate discussion here.

The answer may lie with magnetohydrodynamic effects. To date, most detailed studies of magnetorotational instability have emphasized the production of turbulence rather than high-Q global oscillations, but we suspect that this is the most promising direction for future work.

L.-X. L. and R. N. thank the Institute for Advanced Study and the Department of Astrophysical Sciences, Princeton, for hospitality while part of this work was being done. The research of L.-X. L. was supported by NASA through Chandra Postdoctoral Fellowship grant PF1-20018 awarded by the Chandra X-Ray Center, which is operated by the Smithsonian Astrophysical Observatory for NASA under contract NAS 8-39073. The research of R. N. was supported in part by NSF grant AST 98-20686 and NASA grant NAG 5-10780, and the research of J. G. was supported by NASA grants NAG 5-8385 and NAG 5-1164.

APPENDIX A

THE SHEARING SHEET MODEL

In this appendix we approximate a differentially rotating thin disk by means of the shearing sheet, which consists of a uniform shear flow with a Coriolis force (NGG). We use a Cartesian coordinate system (x, y, z), where x and y are related to the polar coordinates r and ϕ of the original disk by

$$x = r - r_c, \qquad y = r_c(\phi - \Omega_c t) \ . \tag{A1}$$

Here r_c is a reference radius and $\Omega_c = \Omega(r_c)$ is the disk angular velocity at r_c. The velocity of the unperturbed flow is $\boldsymbol{v} = 2Ax\boldsymbol{j}$, where $\boldsymbol{j}$ is a unit vector in the y-direction. The frequency A and the related frequency B are the Oort constants of the disk at r_c:

$$A \equiv \frac{r}{2}\frac{d\Omega}{dr}\bigg|_{r=r_c}, \qquad B \equiv \frac{1}{2r}\frac{d}{dr}\left(r^2\Omega\right)\bigg|_{r=r_c} . \tag{A2}$$

The epicyclic frequency of the flow in the (x, y)-plane is

$$\kappa \equiv \sqrt{4B\Omega_c} = \sqrt{4B(B - A)} \ . \tag{A3}$$

We treat the frequencies A, B, and κ as constants.

When $\Omega \propto r^{-q}$, where q is a constant, we have $2A = -q\Omega_c$, $2B = (2 - q)\Omega_c$, and $\kappa = \sqrt{2(2 - q)}\Omega_c$. It is useful to remark that $q = 2$ corresponds to a disk with constant angular momentum, $q = 3/2$ to a thin Keplerian disk, and $q = 1$ to a disk with constant circular velocity. For $0 < q \leq 2$, we have $A < 0$ and $B \geq 0$.

We assume that the flow is isothermal with an equation of state $p = \rho c_s^2$, where p is the gas pressure, ρ is the mass density, and $c_s = \text{const}$ is the sound speed. We take the flow to be homogeneous and to extend to $\pm\infty$ along x and y. In the vertical

direction we make the usual harmonic approximation for the potential, with vertical frequency $\Omega_\perp$. Then, vertical hydrostatic equilibrium implies $p \propto \rho \propto \exp(-z^2/2h^2)$, where the vertical scale height h is equal to $c_s/\Omega_\perp$. In a thin Keplerian disk, $\Omega_\perp = \Omega_c = \kappa$, but we allow these three frequencies to be different.

Without loss of generality, we assume linear perturbations proportional to $\exp[i(-\omega t + k_y y)]$, where $k_y = m/r_c$ is the azimuthal wavevector and the frequency ω may in general be complex. Then, the first-order perturbation equations are

$$\frac{\partial u}{\partial x} + ik_y v + \frac{1}{\rho_0}\frac{\partial}{\partial z}(\rho_0 w) = \frac{i\sigma}{c_s^2} Q \,, \tag{A4}$$

$$i\sigma u + 2\Omega_c v = \frac{\partial Q}{\partial x} \,, \tag{A5}$$

$$2Bu - i\sigma v = -ik_y Q \,, \tag{A6}$$

$$i\sigma w = \frac{\partial Q}{\partial z} \,, \tag{A7}$$

where u, v, and w are the perturbations to the velocities in the x, y, and z directions, respectively, ρ_0 is the unperturbed mass density, $Q \equiv \delta p/\rho_0$ is the perturbed enthalpy, and

$$\sigma \equiv \omega - m\Omega(r) = -2k_y A x \tag{A8}$$

is the pattern frequency of the mode, where we have chosen r_c to be the corotation radius where the fluid moves with the same speed as the pattern speed of the mode

$$m\Omega(r_c) = \omega \,. \tag{A9}$$

Equations (A4)–(A7) correspond to equations (8) and (10)–(12) for the case of a thin disk, respectively.

From equations (A4)–(A7) a second-order partial differential equation in x and z may be derived for any of the perturbed flow quantities. Following Kato (2002), we consider the equation for Q. The isothermal equation of state allows a separation of variables, $Q = Q_x(x) H_n(z/\sqrt{2}h)$, where $H_n(\eta)$ is a Hermite polynomial of degree $n \geq 0$ (for details see Okazaki et al. 1987; Kato 2002). The function $Q_x(x)$ then satisfies the following differential equation:

$$\frac{d}{dx}\left(\frac{1}{D}\frac{dQ_x}{dx}\right) + \left(\frac{n\Omega_\perp^2 - \sigma^2}{c_s^2\sigma^2} - \frac{k_y^2}{D} - \frac{2k_y\Omega_c}{\sigma}\frac{d}{dx}\frac{1}{D}\right) Q_x = 0 \,, \tag{A10}$$

where $D \equiv \kappa^2 - \sigma^2$. Equation (A10) is similar to equation (16), which we derived for the thin disk. In the same way, we can define a conserved current by

$$J \equiv \frac{i}{2D}\left(Q_x^* \frac{dQ_x}{dx} - Q_x \frac{dQ_x^*}{dx}\right) . \tag{A11}$$

As in a thin disk, there are two types of singularities in equation (A10): the Lindblad singularity at $D = 0$, and the corotation singularity at $\sigma = 0$. The Lindblad singularity is always an apparent singularity. The corotation singularity is a true singularity when $n > 0$ but apparent when $n = 0$. In the WKB limit, there are four permitted regions in a shearing sheet flow when $n > 0$: region I with $\sigma < -\max(\sqrt{n}\Omega_\perp, \kappa)$, region II with $\sigma > \max(\sqrt{n}\Omega_\perp, \kappa)$, region III with $-\min(\sqrt{n}\Omega_\perp, \kappa) < \sigma < 0$, and region IV with $0 < \sigma < \min(\sqrt{n}\Omega_\perp, \kappa)$. Region I (II) and region III (IV) are separated from each other by a potential barrier; region III and region IV are separated from each other by the corotation singularity. When $n = 0$, there are only two permitted regions: I and II.

The results in the main text can be applied to the shearing sheet model. In particular, when $n = 0$, the potential barrier between regions I and II behaves as an amplifier, and a wave incident on it is reflected with larger amplitude (NGG). When $n > 0$, the two potential barriers (one between regions I and III and the other between regions II and IV) behave as a deamplifier, and a wave incident on it is reflected with smaller amplitude. In addition, when $n > 0$, the corotation singularity absorbs energy from a wave.

Here we show some numerical results for the shearing sheet model to confirm these results. Since these numerical solutions do not require that the WKB approximation be valid in regions III and IV, they complement the results obtained in the main text.

For numerical work, it is convenient to replace equation (A10) with an equivalent set of two first-order differential equations. Assuming as before that all variables depend on z as Hermite polynomials $H_n(z/\sqrt{2}h)$ or its derivative, we eliminate w and v from equations (A4)–(A7) to obtain, in matrix form,

$$\frac{d}{dx}\begin{bmatrix} u_x \\ Q_x \end{bmatrix} = \frac{1}{\sigma}\begin{bmatrix} -2k_y B & \dfrac{i(\sigma^2 - n\Omega_\perp^2 - k_y^2 c_s^2)}{c_s^2} \\ i(\sigma^2 - \kappa^2) & 2k_y\Omega_c \end{bmatrix}\begin{bmatrix} u_x \\ Q_x \end{bmatrix} . \tag{A12}$$

In this first-order form of the linearized equations, it is clear that the only possible singularity is $\sigma = 0$. This explains why the Lindblad resonances $\sigma = \pm\kappa$ are not true singularities of the equivalent second-order equations (A10) and (16).

We look for solutions to equation (A12) that contain only outgoing waves in region II. To do so, we start from an outgoing wave at $x_0 > 0$ in the WKB region II, which has a positive wavevector (thus a positive group velocity), and then integrate the equations along the real axis of $+x$ toward the corotation. Near but before crossing the corotation, we deform the integration path into the complex plane of x to pass the corotation singularity from above and then come back to the real axis of $-x$. Then, we integrate the equations along the real axis of $-x$ into the WKB region I, until $x = -x_0$ is reached. At $x = -x_0$, we decompose the solution into an ingoing component (having a negative wavevector, i.e., a positive group velocity) and an outgoing component (having a positive wavevector, i.e., a negative group velocity). Then, we calculate the gain G (i.e., the reflection coefficient) and the transmission coefficient T by

$$G = \left|\frac{u_{x,\mathrm{out}}(x=-x_0)}{u_{x,\mathrm{in}}(x=-x_0)}\right|^2 = \left|\frac{Q_{x,\mathrm{out}}(x=-x_0)}{Q_{x,\mathrm{in}}(x=-x_0)}\right|^2 , \tag{A13}$$

$$T = \left|\frac{u_{x,\mathrm{out}}(x=x_0)}{u_{x,\mathrm{in}}(x=-x_0)}\right|^2 = \left|\frac{Q_{x,\mathrm{out}}(x=x_0)}{Q_{x,\mathrm{in}}(x=-x_0)}\right|^2 , \tag{A14}$$

where "out" denotes "outgoing" and "in" denotes "ingoing."

Numerical results corresponding to a few choices of parameters are shown in Table 2. They are classified into two classes: one with $n = 0$ and the other with $n = 1$. Each class contains both a Keplerian disk ($\Omega_\perp = \kappa = \Omega_c$) and non-Keplerian disks ($\Omega_\perp$ and κ different from Ω_c). The results show that, for the case of $n = 0$, where the corotation is not an intrinsic singularity, the incident wave is amplified: $G > 1$; indeed, $G = 1 + T$ since the current is conserved. One can check that the numerical results agree with the analytical results of NGG, where

$$G = 1 + T = 1 + \exp(-2\pi C), \qquad C = \frac{c_s^2 k_y^2 + \kappa^2}{4c_s|Ak_y|} . \tag{A15}$$

However, for the case of $n = 1$, where the corotation is an intrinsic singularity, there is strong absorption at the corotation as indicated by the fact that $T \ll 1 - G$, and the incident wave is always deamplified since $G < 1$.

The initial and terminal points of our numerical integrations are always chosen well within the WKB domain of regions II and I, respectively (i.e., $|k_x x| \gg 1$, where k_x is the wavevector in the x-direction), so that the ingoing and outgoing waves are clearly distinguishable. It can be shown that for $n \geq 1$, the criterion for the validity of the WKB approximation in regions III and IV near corotation reduces to $b \gg 1$, where

$$b \equiv \frac{\kappa}{-2Ak_y h} .$$

The solutions listed in Table 2 do not satisfy $b \gg 1$. Indeed, for the last solution, where $\Omega_\perp = 0.8\Omega_c$, $\kappa = 0.2\Omega_c$, and $k_y h = 0.3$, we have $b = 0.336$ and $q = \frac{1}{2}(nb^2 - \frac{1}{4})^{1/2} = 0.185i$. Even for this case with an imaginary q, we see that $T < 1 - G$, which must be attributed to absorption at corotation. These numerical results support and complement our analytical results based on the WKB approximation.

APPENDIX B

STRATIFIED SHEAR FLOWS

Subsonic stratified shear flows are often important in the atmosphere and in the ocean, for example, a horizontal velocity $\boldsymbol{V} = V_x(z)\boldsymbol{e}_x$ and density $\rho_{\mathrm{water}}(z)$ or entropy $S_{\mathrm{air}}(z)$ that vary with height z. Waves may exist in such flows and suffer resonant absorption directly analogous to what we have demonstrated for disk g-modes. Such terrestrial flows are *stably stratified* if the Brunt-Väisälä frequency

$$N \equiv \left(-g\frac{d\ln\rho}{dz}\right)^{1/2} \tag{B1}$$

is real, where g is the acceleration of gravity (9.8 m s^{-2}), and $\ln\rho$ should be replaced with $(\gamma^{-1} - 1)S/k_{\mathrm{B}}$ for a compressible fluid, such as the atmosphere. While $N^2 > 0$ ensures stability against convection, shear instabilities may still occur.

In the Boussinesq approximation (i.e., neglecting $\delta\rho$ except in buoyancy terms), vertical velocity perturbations $\delta V_z(t, x, z) = v(z)\exp(ik_x x - i\omega t)$ satisfy the Taylor-Goldstein equation (e.g., Drazin & Reid 1981),

$$\frac{d^2 v}{dz^2} + \left[\frac{N^2(z)}{(\omega - k_x V_x)^2} + \frac{V_x''(z)}{k_x(\omega - k_x V_x)} - 1\right]k_x^2 v = 0 . \tag{B2}$$

The equation is singular at any depth z_c where the unperturbed current matches the horizontal phase velocity of the disturbance, $V_x(z_c) = \omega/k_x$; such depths are called *critical layers* and are analogous to corotation radii in disks.

A good deal is known about the instabilities of the Taylor-Goldstein equation for standard boundary conditions, e.g., $v = 0$ or $dv/dz = 0$ (for details see Drazin & Reid 1981). If $N^2 = 0$ so that the most singular term vanishes, a necessary condition for

instability is that V_x'' must change sign within the flow (Rayleigh's Inflection Point Theorem). In addition, there are no growing modes—in fact, no modes at all—if $V_x'' = 0$ throughout the flow (Case 1960). The term analogous to V_x'' in disks is $d(\kappa^2/2\Omega\Sigma)/dr$, which vanishes throughout the shearing sheet. Where they occur, the Taylor-Goldstein instabilities are of Kelvin-Helmholtz type, and marginally unstable modes have their critical layers at the inflection point. If $N^2 > 0$, it is necessary for instability that the *Richardson number*

$$R \equiv \left(\frac{N}{V_x'}\right)^2 \tag{B3}$$

be less than $\frac{1}{4}$ somewhere within the flow. This can be understood qualitatively by comparing the kinetic energy available from the shear with the gravitational potential energy that must be overcome when fluid elements from different depths are brought together. Howard (1961) gave a short proof, which is worth sketching because it applies at least in part to equation (16). Writing $\sigma(z) = \omega - k_x V_x$ and defining $v = \varphi\sqrt{\sigma}$, equation (B2) can be recast as

$$(\sigma\varphi')' + k_x^2\left[\frac{N^2 - (1/4)(V_x')^2}{\sigma} - \sigma + \frac{V_x''}{2k_x}\right]\varphi = 0\,.$$

Multiplying by the complex conjugate variable φ^* and integrating over the whole flow yields

$$\int_{z_1}^{z_2}\left\{\sigma|\varphi'|^2 + k_x^2\left[\frac{(1/4)(V_x')^2 - N^2}{\sigma} + \sigma - \frac{V_x''}{2k_x}\right]|\varphi|^2\right\}dz = \sigma\varphi^*\varphi'\Big|_{z_1}^{z_2}\,.$$

The integrated term on the right-hand side obviously vanishes if $v = 0$ at z_1, z_2, and with a little more effort, it can be seen to be real if $dv/dz = 0$ at the boundaries. Therefore, the imaginary part of the last equation is

$$\omega_I \int_{z_1}^{z_2}\left\{|\varphi'|^2 + k_x^2\left[\frac{N^2 - (1/4)(V_x')^2}{|\sigma|^2} + 1\right]|\varphi|^2\right\}dz = 0\,. \tag{B4}$$

The integral is positive if $R \geq \frac{1}{4}$ everywhere, whence $\omega_I = 0$.

Booker & Bretherton (1967) studied a forced, initial-value version of this problem. A weak source term $\propto\exp(ik_x x - i\omega t)$ and localized in z commences at $t = 0$ and continues indefinitely (ω is real). The resulting wave train propagates toward its critical layer $z = z_c$. As $t \to \infty$, the wave energy within any finite interval around z_c increases $\propto t$ without bound (viscosity and nonlinearity being neglected). Booker & Bretherton (1967) explained this by noting that in the WKB approximation, the group velocity scales as $(z - z_c)^2$ so that the propagation time from the source to the critical layer is infinite. They also showed, however, that the wave train on the side of the critical layer opposite the source does not vanish at late times but is reduced in amplitude by a factor

$$\exp\left(-\pi\sqrt{R - \frac{1}{4}}\right) \tag{B5}$$

if $R > \frac{1}{4}$. These results justify the view that the corotation or critical-layer resonance is an absorber of wave energy, even in an inviscid flow.

What does all this have to do with the disk oscillations? Near $\sigma = 0$, the largest terms in equation (16) or equation (A10) have the same form as those in the Taylor-Goldstein equation (B2). The analog to N^2 is $n\kappa^2/(mh/r)^2$. Hence, our analog of the Richardson number is

$$R_\kappa = \frac{n}{(mh/r)^2}\frac{\kappa^2}{(2A)^2} = nb^2\,. \tag{B6}$$

Just as N^2 measures stratification of density (or entropy) in a gravitational field, so κ^2 measures radial "stratification" of angular momentum per unit mass. Although the mathematical consequences of the singularities associated with R and R_κ are similar, R_κ depends on the streamwise wavenumber (m/r or k_y).

These differences are related to the physical nature of fluid oscillations near resonance. In the case of the Taylor-Goldstein equation, the restoring force is buoyancy and the oscillations are closely related to geophysical internal waves and stellar oscillations. If $\boldsymbol{N}$ is a vectorial form of the Brunt-Väisälä frequency with direction parallel to the gravitational field, the local three-dimensional WKB dispersion relation is

$$\sigma^2 = \frac{(\boldsymbol{N}\times\boldsymbol{k})^2}{k^2}\,, \tag{B7}$$

where $k = (\boldsymbol{k}\cdot\boldsymbol{k})^{1/2}$ is the total wavenumber and σ is the wave frequency in the local rest frame of the fluid. Waves are transverse, $\boldsymbol{k}\cdot\delta\boldsymbol{v} = 0$, since $\nabla\cdot\delta\boldsymbol{v} \approx 0$. If $\boldsymbol{k}$ is parallel to $\boldsymbol{N}$, then displacements are horizontal, the restoring force of buoyancy vanishes, and $\sigma \to 0$. As the wave approaches the critical layer, $\boldsymbol{k}$ tries to align with $\boldsymbol{N}$ (i.e., along z); since the component k_x is fixed, this forces $k_z \approx \pm k_x N/\sigma \to \infty$, and the vertical group velocity $v_{gz} = (\partial k_z/\partial\sigma)^{-1} = \mp\sigma^2/Nk_x \to 0$.

In our disk problem, the restoring force near corotation depends on stratification of angular momentum rather than entropy, so that waves are essentially inertial oscillations:

$$\sigma^2 = \frac{(\boldsymbol{\kappa}\cdot\boldsymbol{k})^2}{k^2} \rightarrow \frac{\kappa^2 n/h^2}{k_r^2 + n/h^2 + (m/r)^2}\,, \tag{B8}$$

where $\boldsymbol{\kappa}$ is parallel to the rotation axis and we have identified $\sqrt{n}/h$ as the vertical wavenumber (see eq. [17]). In a uniformly rotating fluid, equation (B8) reduces to $(2\boldsymbol{\Omega}\cdot\boldsymbol{k})^2/k^2$ (e.g., Greenspan 1968). The gradient of the pressure perturbation, being parallel to $\boldsymbol{k}$, does no work but enforces the constraint $\boldsymbol{k}\cdot\delta\boldsymbol{v} = 0$. Thus, within planes perpendicular to $\boldsymbol{k}$, the fluid moves as if in free epicycles but with reduced frequency because the angular momentum gradient has to be projected onto these planes. There is an analogy here with the geophysical principle that the Coriolis force acting on large-scale atmospheric motions, which are horizontal by necessity, is reduced by the sine of latitude (Pedlosky 1987).

As corotation is approached, $\boldsymbol{k}$ wants to be perpendicular to $\boldsymbol{\kappa}$, i.e., horizontal, so that $\sigma \rightarrow 0$ (eq. [B8]). Since the vertical component of the wavenumber is fixed, however, $\boldsymbol{k}$ becomes horizontal only if $k_r \rightarrow \infty$ ($n > 0$). Very close to corotation, $\sigma \propto k_r^{-1}$ so that the radial group velocity $\partial\sigma/\partial k_r$ vanishes as $(r - r_c)^2$. Therefore, as in the case analyzed by Booker & Bretherton (1967), wave packets cannot reach $\sigma = 0$ in finite time. This WKB reasoning presumes $k_r|r - r_c| \gg 1$, which is equivalent to $\sqrt{R_\kappa} \gg 1$. As in the Taylor-Goldstein case, our more precise analysis reveals an exponentially small penetration through corotation.

REFERENCES

Abramowicz, M. A., & Kluzniak, W. 2001, A&A, 374, L19
Bate, M. R., Ogilvie, G. I., Lubow, S. H., & Pringle, J. E. 2002, MNRAS, 332, 575
Blaes, O. M. 1987, MNRAS, 227, 975
Booker, J. R., & Bretherton, F. P. 1967, J. Fluid Mech., 27, 513
Case, K. 1960, Phys. Fluids, 3, 143
Drazin, P. G., & Reid, W. H. 1981, Hydrodynamic Stability (Cambridge: Cambridge Univ. Press)
Goldreich, P., & Narayan, R. 1985, MNRAS, 213, 7P (GN)
Greenspan, H. P. 1968, Theory of Rotating Fluids (Cambridge: Cambridge Univ. Press)
Howard, L. N. 1961, J. Fluid Mech., 10, 509
Kato, S. 2001a, PASJ, 53, 1
———. 2001b, PASJ, 53, L37
———. 2002, PASJ, 54, 39
———. 2003, PASJ, 55, 257
Kato, S., Fukue, J., & Mineshige, S. 1998, Black Hole Accretion Disks (Kyoto: Kyoto Univ. Press)
Mark, J. W. K. 1976, ApJ, 205, 363
Merzbacher, E. 1998, Quantum Mechanics (New York: Wiley)
Narayan, R., Goldreich, P., & Goodman, J. 1987, MNRAS, 228, 1 (NGG)
Nowak, M. A., & Wagoner, R. V. 1991, ApJ, 378, 656
———. 1992, ApJ, 393, 697
Nowak, M. A., Wagoner, R. V., Begelman, M. C., & Lehr, D. E. 1997, ApJ, 477, L91
Okazaki, A. T., Kato, S., & Fukue, J. 1987, PASJ, 39, 457
Ortega-Rodriguez, M., & Wagoner, R. V. 2000, ApJ, 537, 922
Pedlosky, J. 1987, Geophysical Fluid Dynamics (New York: Springer)
Perez, C. A., Silbergleit, A. S., Wagoner, R. V., & Lehr, D. E. 1997, ApJ, 476, 589
Remillard, R. A., Muno, M. P., McClintock, J. E., & Orosz, J. A. 2002, preprint (astro-ph/0208402)
Silbergleit, A., Wagoner, R. V., & Ortega-Rodríguez, M. 2001, ApJ, 548, 335
Stella, L., & Vietri, M. 1998, ApJ, 492, L59
Stella, L., Vietri, M., & Morsink, S. M. 1999, ApJ, 524, L63
van der Klis, M. 2000, ARA&A, 38, 717
Wagoner, R. V. 1999, Phys. Rep., 311, 259
Wagoner, R. V., Silbergleit, A. S., & Ortega-Rodriguez, M. 2001, ApJ, 559, L25
Yavneh, I., McWilliams, J. C., & Molemaker, M. J. 2001, J. Fluid Mech., 448, 1

Note added in proof.—Notwithstanding the argument in § 3.2, there can be a logarithmic singularity in dQ_r/dr at corotation even for $n = 0$. This depends on gradients in the disk on the scale of r, so it is weak compared to the singularity for $n > 0$ and does not appear in the shearing sheet.